NASA Technical Memorandum 103668
ICOMP-90-25

The Effect of Small Streamwise Velocity Distortion on the Boundary Layer Flow Over a Thin Flat Plate With Application to Boundary Layer Stability Theory

M.E. Goldstein
Lewis Research Center
Cleveland, Ohio

S.J. Leib
Sverdrup Technology, Inc.
Lewis Research Center Group
Brook Park, Ohio

and

S.J. Cowley
University of Cambridge
Cambridge, England

and Institute for Computational Mechanics in Propulsion
Lewis Research Center
Cleveland, Ohio

December 1990

NASA

THE EFFECT OF SMALL STREAMWISE VELOCITY DISTORTION ON THE BOUNDARY LAYER FLOW OVER A THIN FLAT PLATE WITH APPLICATION TO BOUNDARY LAYER STABILITY THEORY

M.E. Goldstein
National Aeronautics and Space Administration
Lewis Research Center
Cleveland, Ohio 44135

S.J. Leib
Sverdrup Technology, Inc.
Lewis Research Center Group
Brook Park, Ohio 44142

and

S.J. Cowley
University of Cambridge
DAMTP, Silver St.
Cambridge CB39EW, England

and Institute for Computational Mechanics in Propulsion
Lewis Research Center
Cleveland, Ohio 44135

E-5759-1

ABSTRACT

We show how an initially linear spanwise disturbance of the free-stream velocity field is amplified by leading edge bluntness effects and ultimately leads to a small amplitude but nonlinear spanwise motion far downstream from the edge. This spanwise motion is imposed on the boundary layer flow and ultimately causes an order-one change in its profile shape. The modified profiles are highly unstable and can support Tollmein-Schlichting wave growth well upstream of the theoretical lower branch of the neutral stability curve for a Blasius boundary layer.

1. INTRODUCTION

Efforts to understand boundary layer transition have been underway for a number of years now. The relevant experimental measurements are usually made on the boundary layer flows over relatively thin flat plates embedded in nominally uniform free streams. The final turbulent state arises from the relatively slow streamwise growth of initially linear instability waves that gradually evolve from the small amplitude unsteadiness that either occurs naturally in the experiments or can be artificially imposed by the experimenter in order to organize the motion.

An important unresolved issue involves the observed instability wave growth that occurs upstream of the theoretical (i.e., two-dimensional flat plate) lower branch of the neutral stability curve in some experiments. One purpose of the present paper is to provide a possible explanation of this phenomena. We show that small but steady variations in the upstream velocity

field can produce somewhat larger streamwise vorticity fields within the boundary layer which can, in turn, produce significant (i.e., order-one) variations in the streamwise boundary layer profiles. These profiles turn out to be non-inflectional and therefore incapable of supporting rapidly growing inviscid instabilities with growth rates that scale with the inverse boundary layer thickness. However, the local wall shear becomes small at certain spanwise locations which tends to move the lower branch of the Tollmein-Schlichting wave neutral stability curve upstream of its theoretical flat plate location. The streamwise vorticity field can also amplify the Tollmein-Schlichting waves through the resonant mechanism suggested by Nayfeh (1981). The resulting three-dimensional disturbances would then grow on the inverse spanwise length scale of the disturbance which could (numerically if not asymptotically) be equal to the Tollmein-Schlichting wave growth rates.

Goldstein (1983) and Goldstein et al. (1983) showed that long wavelength free-stream disturbances can interact with the rapidly developing leading edge boundary layer to generate spatially decaying asymptotic eigenmodes that eventually turn into spatially amplified Tollmein-Schlichting waves once they reach the lower branch of the neutral stability curve. The present analysis shows that small nonuniformities in the oncoming stream can cause the relevant branch to move well upstream of its theoretical Blasius location.

Crow (1966) also considered the steady distortion of flat-plate boundary layer flows by free stream nonuniformities, but that work is quite different from ours. One important difference is that the present work is concerned with the augmentation of instability wave growth while Crow is concerned with the development of three dimensionality. Our emphasis is therefore on the linear and nonlinear amplification mechanisms that ultimately produce order-one changes in the boundary layer flow, while the boundary layer flow is linearized about the Blasius flow in the Crow analysis. In this regard, it is worth noting that leading-edge bluntness effects play a central role in the present work, while Crow considers only an infinitely thin flat plate. Another important difference is that the present work qualitatively predicts the destabilization of the boundary layer flow, while Crow's analysis, which is only concerned with the three dimensionality, does not.

We assume that the dimensions of the 'leading edge ellipse' are of the order of the spanwise length scale, say λ, of the upstream disturbance field and that the Reynolds number based on λ, say R_λ, is large. Then the upstream distortion interacts linearly with the leading edge with the resulting flow being well described by the usual 'rapid distortion' theory (Hunt and Carruthers, 1990, and Goldstein, 1978). The relevant analysis was, at least in principle, given by Lighthill (1956) who showed that the upstream distortion produces a cross flow velocity field that becomes logarithmically infinite at the surface of the plate. The logarithmic singularity must ultimately be removed by viscous effects, which (as in Toomre, 1960) are confined to the viscous boundary layer region (with the Reynolds number - amplitude scaling being considered herein). Our analysis shows that the inviscid cross flow effects produce only a linear perturbation of the boundary layer flow in the vicinity of the leading edge, where the undisturbed boundary layer undergoes its most rapid streamwise development, but that they produce an order-one change in the mean boundary layer profiles at large distances downstream where its streamwise development is on a considerably slower scale.

However, the linear rapid distortion theory solution, which provides an adequate description of the external inviscid flow in the vicinity of the leading edge, begins to break down at large streamwise distances with the breakdown moving further upstream as the surface of the plate is approached. A new nonlinear solution then has to be obtained in order to describe the inviscid flow outside the boundary layer in the physically interesting region where cross flow effects produce a significant (i.e., order-one) profile change. The thickness of this nonlinear inviscid region is small compared to its streamwise dimension but large compared to the boundary layer thickness. It serves as a kind of 'blending layer' that connects the boundary layer solution to the linear rapid distortion theory solution, which applies at an order-one (on the scale of λ) distance from the wall.

The blending layer flow is governed by the nonlinear 'water wave' equation whose solution eventually develops a singularity at a certain spanwise location and at a finite downstream position due to the well-known wave steeping effects associated with that solution. This also produces a singularity (signified by the vanishing of the wall shear) in the boundary layer flow at the same (spanwise and streamwise) location. The boundary layer therefore, develops localized regions of relatively small spanwise extent in which the flow is destabilized as a result of large reductions in the wall shear.

New local solutions to the blending and boundary layer problem have to be worked out in order to understand the structure of these regions. The two solutions must then be matched in an appropriate overlap domain. The boundary layer solution actually develops a double layer structure as it approaches the singularity so that the overall asymptotic structure has three layers in the vicinity of the singularity. A second purpose of this paper is to investigate the relevant structure of this local solution.

The overall plan of the paper is as follows. Section 2.1 describes the linear inviscid flow produced by the steady upstream distortion field and the initial breakdown of the relevant linear 'rapid distortion' theory solution is discussed in section 2.2. The appropriate nonlinear, but inviscid, solution that eliminates the breakdown is described in section 3. In section 4 we show that this solution develops a singularity somewhat further downstream and that this singularity can, in turn, be eliminated by a new local solution to the problem.

The viscous boundary layer problem is formulated in section 5. The solution to this problem develops a singularity at the position of the inviscid singularity and the terminal form of the boundary layer solution is worked out in section 5.2. This local similarity solution has a double layer structure with an outer inviscid region and a viscous wall layer. A new expansion which continues the boundary layer solution through the singularity is worked out in sections 5.3 and 5.4. This solution has the same streamwise length scale as the external solution and it is shown that the two solutions can be matched in an appropriate overlap domain.

The numerical solutions to the boundary layer problem are described in section 6. They show that it exhibits a rapid thickening in the vicinity of the singularity, which might be characterized as a kind of "bursting" of the boundary layer - a phenomena which has, up to now, been found only in unsteady

flows. This might lead to a local transition of the boundary layer and therefore provide a possible mechanism for by-pass transition. These and other issues are discussed in section 7.

2. FORMULATION AND BREAKDOWN OF LINEAR SOLUTION

We are concerned with the flow over a semi-infinite flat plate of finite thickness t^* and a leading edge 'ellipse' whose dimensions are also $O(t^*)$ (see fig. 1). The upstream flow is assumed to be nominally uniform, except for a small $O(\varepsilon)$ steady perturbation, say $\varepsilon U_\infty u_\infty(z)$, in the streamwise velocity that depends only on the spanwise coordinate λz and has a characteristic length scale λ. $u_\infty(z)$ is, of course, an order-one quantity. We suppose that all lengths have been normalized by λ and that the velocity $\vec{u} = \{u,v,w\}$ has been normalized by the uniform upstream mean flow velocity U_∞. The flow is assumed to be incompressible, with density ρ, and the pressure p is normalized by ρU_∞^2. The plate thickness t^* is taken to be $O(\lambda)$, and the x-coordinate is assumed to be in the streamwise direction with the origin at the leading edge while the origin of the y-coordinate is at the flat surface of the plate far downstream in the flow.

Finally, we require that the Reynolds number $R_\lambda = U_\infty\lambda/\nu$, where ν is the kinematic viscosity, be large enough to insure that the viscous effects are confined to a narrow boundary layer at the surface the plate that is predominantly two dimensional near the forward stagnation point. This will occur if

$$\ln R_\lambda \ll \frac{1}{\varepsilon} \ll R_2 \ , \tag{2.1}$$

which we now assume to be the case.

2.1. The Linear Solution

The entire flow is then two dimensional in the vicinity of the leading edge, i.e., in the region where $x = O(1)$, with the three-dimensional effects being an $O(\varepsilon)$ perturbation of the two-dimensional base flow, say $\{U_0(x,y), V_0(x,y),0\}$. The viscous effects are confined to a narrow region whose thickness is $O\left(R_\lambda^{-1/2}\right)$. The solution outside this region should therefore expand like

$$\vec{u} = \{U_0,V_0,0\} + \varepsilon\{u_0,v_0,w_0\} + \varepsilon^2\{u_1,v_1,w_1\} + \ldots = \{U_0,V_0,0\} + \varepsilon\vec{u}_0 + \varepsilon^2\vec{u}_1 + \ldots \tag{2.2}$$

and

$$p = P_0 + \varepsilon p_0 + \varepsilon^2 p_1 + \ldots \ . \tag{2.3}$$

The complex conjugate mean flow velocity $\zeta = U_0 - iV_0$ is an analytic function of $Z = x + i[y + (t^*/\lambda)]$ that can be expressed in terms of a complex potential, say

$$\tilde{W} = \Phi + i\Psi \ , \tag{2.4}$$

where Φ is the velocity potential and Ψ is the stream function, in the usual way by

$$\zeta = \frac{d\tilde{W}}{dZ} \ . \tag{2.5}$$

For definiteness, we suppose that $\Psi = 0$ on the surface of the (body) plate and along the stagnation streamline and that $\Phi \to 0$ at the forward stagnation point.

The first order perturbations are governed by the linearized Euler equations and the results obtained by Goldstein (1978) (also see Goldstein, 1979) can easily be specialized to the present case to show that the relevant solution can be written as

$$\vec{u}_0 = \nabla\phi + u_\infty(z)\nabla\,\Delta(x,y) \ , \tag{2.6}$$

$$p_0 = -\left(U_0\,\frac{\partial}{\partial x} + V_0\,\frac{\partial}{\partial y}\right)\phi \ , \tag{2.7}$$

where

$$\nabla^2\phi = -u_\infty(z)\nabla^2\,\Delta \ , \tag{2.8}$$

$$\Delta = \Phi + \int_{-\infty}^{\Phi}\left[\frac{1}{U_0^2(\Psi,\Phi) + V_0^2(\Psi,\Phi)} - 1\right]d\Phi \tag{2.9}$$

is the Lighthill (1956) - Darwin (1954) drift function and the normal component of $\vec{u}_0$ must vanish at the surface of the plate.

2.2. Breakdown of the Linear Solution

The expansion (2.1) is nonuniform in the vicinity of the plate. In fact, it is easy to show from these equations, along with the results of Appendix A, that the cross flow velocity w_0 becomes infinite there like

$$w_0 \to \frac{u_\infty'(z)}{a}\ln\Psi \qquad \text{as} \qquad \Psi \to 0 \tag{2.10}$$

where a is a constant related to the local potential flow behavior in the vicinity of the forward stagnation point and the prime denotes differentiation

with respect to z (also see Lighthill, 1956). The remaining velocity components, as well as the pressure, remain finite. The strongest nonuniformity occurs in the stagnation point region where the mean flow goes to zero. In fact, it is easily shown from the results of Appendix A that εp_0 becomes of the same order as P_0 at an $O(\varepsilon^{1/2})$ distance from this point. However, the linearized equations still give the correct solution (to the order of interest here) right up to the edge of the viscous boundary layer and this nonuniformity need not be considered further.

However, another, much more important, nonuniformity develops far downstream in the flow where x becomes large. To understand its structure we note that

$$\Psi \to y, \; U_0 \to 1, \; \Phi \to x, \; \Delta \to \Delta_+(y) + x \qquad \text{as} \qquad x \to \infty \; , \tag{2.11}$$

where

$$\Delta_+(y) = \int_{-\infty}^{\infty} \left(\frac{1}{U_0^2 + V_0^2} - 1 \right) d\Phi \to \Delta_0(y) - \frac{1}{a} \ln y \qquad \text{as} \qquad y \to 0 \tag{2.12}$$

and Δ_0 remains bounded.

It is now convenient to introduce the new dependent variable

$$\tilde{\phi} \equiv \phi + u_\infty(z)\Delta_+(y) \tag{2.13}$$

Equations (2.6) and (2.8) then show that

$$\nabla^2 \tilde{\phi} = u_\infty'' \Delta_+ \; , \tag{2.14}$$

and the normal component of $\vec{u}_0$ will vanish at the plate if

$$\frac{\partial \tilde{\phi}}{\partial y} = 0 \qquad \text{at} \qquad y = 0 \; . \tag{2.15}$$

It now follows from (2.12), (2.13), and (2.15) that $\tilde{\phi}$ becomes independent of x and, consequently, that (see (2.7))

$$\vec{u}_0 \to \left(u_\infty, \frac{\partial \tilde{\phi}}{\partial y}, \frac{\partial \tilde{\phi}}{\partial z} - u_\infty' \Delta_+ \right) \; , \tag{2.16}$$

$$p_0 \to 0 \; , \tag{2.17}$$

and

$$\tilde{\phi} \to \beta(z) - \frac{u_\infty''}{a}\,\frac{y^2}{2}\,\ln y \qquad \text{as} \qquad y \to 0\ . \tag{2.18}$$

Substituting (2.1) and (2.2) into Euler's equations and using the second member of (2.11) along with (2.14) shows that

$$\frac{\partial \vec{u}_1}{\partial x} + \nabla p_1 \to -\vec{u}_0 \cdot \nabla \vec{u}_0 \to -\left[\tilde{\phi}_y \frac{\partial}{\partial y} + \left(\tilde{\phi}_z - u_\infty' \Delta_+\right) \frac{\partial}{\partial z}\right]\left(u_\infty,\ \tilde{\phi}_y,\ \tilde{\phi}_z - u_\infty' \Delta_+\right)$$

$$\text{as} \qquad x \to \infty\ . \tag{2.19}$$

It therefore follows from (2.12) and (2.18) that

$$\frac{\partial}{\partial x}\,(u_1 + p_1) \to -\frac{u_\infty'^2}{a}\,\ln y\ , \tag{2.20}$$

$$\frac{\partial v_1}{\partial x} + \frac{\partial p_1}{\partial y} \to -\frac{\left(u_\infty''^2 - u_\infty' u_\infty'''\right)}{a^2}\, y\, \ln^2 y\ , \tag{2.21}$$

$$\frac{\partial w_1}{\partial x} + \frac{\partial p_1}{\partial z} \to -\frac{u_\infty' u_\infty''}{a^2}\,\ln^2 y \qquad \text{as} \qquad x \to \infty \quad \text{and} \quad y \to 0\ . \tag{2.22}$$

Then since $\tilde{u}_1$ satisfies the continuity equation

$$\nabla \cdot \vec{u}_1 = 0\ , \tag{2.23}$$

it follows from these results that

$$\nabla^2 p_1 \to -2\left(\frac{u_\infty''}{a}\,\ln y\right)^2 \qquad \text{as} \quad y \to 0 \quad \text{and} \quad x \to \infty \tag{2.24}$$

and, consequently, that

$$p_1 \to d(z) - \left(\frac{u_\infty'' y\, \ln y}{a}\right)^2 \qquad \text{as} \qquad y \to 0 \quad \text{and} \quad x \to \infty\ . \tag{2.25}$$

It now follows from (2.1), (2.2), (2.10), (2.11), and (2.20) to (2.22) that

$$u \to 1 + \varepsilon u_\infty(z) - \frac{\varepsilon^2 x u_\infty'^2}{a}\,\ln y \tag{2.26}$$

$$w \to \frac{\varepsilon u_\infty'}{a} \ln y - \frac{\varepsilon^2 x u_\infty' u_\infty''}{a^2} \ln^2 y \tag{2.27}$$

$$p \to \varepsilon^2 d(z) - \left(\frac{\varepsilon u_\infty'' y \ln y}{a}\right)^2 , \tag{2.28}$$

as $x \to \infty$, $y \to 0$.

It is clear that this linear expansion must break down when

$$-\varepsilon x \ln y = O(1) \tag{2.29}$$

and that a new solution must then be found for this region.

3. BLENDING LAYER SOLUTION

To obtain this solution we anticipate that viscous effect will still be unimportant and introduce the new gauge functions

$$\sigma(\varepsilon) = -\frac{1}{\ln \delta(\varepsilon)} \to 0 \qquad \text{as} \qquad \varepsilon \to 0 , \tag{3.1}$$

to be specified more precisely below, along with the new scaled variables

$$\bar{x} \equiv \frac{\varepsilon x}{\sigma} \tag{3.2}$$

$$\eta \equiv -\sigma \ln y = \frac{\ln y}{\ln \delta} . \tag{3.3}$$

The necessity of using logarithmic variables in problems of this type was pointed out by Lagerstrom and Casten (1972) and by Bush (1971) (see also Agvawal and Messiter, 1984).

We simplify the algebra by using the new independent variables

$$\xi \equiv \bar{x}\eta \tag{3.4}$$

and η in place of $\bar{x}$ and η. Then the Euler and continuity equation becomes

$$\left[\frac{\varepsilon}{\sigma}\eta u \frac{\partial}{\partial \xi} - \sigma v e^{\eta/\sigma}\left(\frac{\partial}{\partial \eta} + \frac{\xi}{\eta}\frac{\partial}{\partial \xi}\right) + w \frac{\partial}{\partial z}\right]\vec{u} = -\left[\frac{\varepsilon}{\sigma}\eta \frac{\partial}{\partial \xi} , -\sigma e^{\eta/\sigma}\left(\frac{\partial}{\partial \eta} + \frac{\xi}{\eta}\frac{\partial}{\partial \xi}\right), \frac{\partial}{\partial z}\right] p , \tag{3.5}$$

and

$$\frac{\varepsilon}{\sigma}\eta \frac{\partial u}{\partial \xi} - \sigma e^{\eta/\sigma}\left(\frac{\partial}{\partial \eta} + \frac{\xi}{\eta}\frac{\partial}{\partial \xi}\right)v + \frac{\partial w}{\partial z} = 0 \tag{3.6}$$

Equations (2.26) to (2.28) suggest that the solution in this region will be of the form

$$u = 1 + \varepsilon \bar{u}_0(\xi, z) \ , \tag{3.7}$$

$$v = \frac{\varepsilon}{\sigma} e^{-\eta/\sigma} \eta \bar{v}_0(\xi, z) \ , \tag{3.8}$$

$$w = \frac{\varepsilon}{\sigma} \eta \bar{w}_0(\xi, z) \ , \tag{3.9}$$

and

$$p = \varepsilon^2 d(z) + \frac{1}{2} \left(\frac{\varepsilon \eta}{\sigma} e^{-\eta/\sigma} \right)^2 \bar{p}_0(\xi, z) \ , \tag{3.10}$$

where $\bar{u}_0$, $\bar{v}_0$, $\bar{w}_0$, and $\bar{p}_0$ are, of course, assumed to remain $O(1)$ in the 'blending layer' limit $\varepsilon \to 0$ with ξ, η, z held fixed.

Substituting these into (3.5) and (3.6) and retaining only lowest order terms, we obtain

$$\frac{\partial \bar{u}_0}{\partial \xi} + \bar{w}_0 \frac{\partial \bar{u}_0}{\partial z} = 0 \tag{3.11}$$

$$\frac{\partial \bar{v}_0}{\partial \xi} + \bar{v}_0^2 + \bar{w}_0 \frac{\partial \bar{v}_0}{\partial z} = -\bar{p}_0 \ , \tag{3.12}$$

$$\frac{\partial \bar{w}_0}{\partial \xi} + \bar{w}_0 \frac{\partial \bar{w}_0}{\partial z} = 0 \ , \tag{3.13}$$

and

$$\bar{v}_0 + \frac{\partial \bar{w}_0}{\partial z} = 0 \ , \tag{3.14}$$

respectively. Equation (3.13) can be solved for $\bar{w}_0$, the result can then be used in (3.14) to determine $\bar{v}_0$, which can, in turn, be used in (3.12) to determine $\bar{p}_0$. Equation (3.11) can, of course, be solved for $\bar{u}_0$.

It is well known that the general solution to the 'water wave type' equation (3.13) can be written implicitly as

$$\bar{w}_0 = F(z - \bar{w}_0 \xi) \ , \tag{3.15}$$

where F is an, as yet, undetermined (arbitrary) function of the indicated argument. This solution must match onto the linear solution (2.27) in the limit as $\eta \to 0$ with $\bar{x}$ fixed and the limit $\bar{x} \to 0$ with η fixed - both of which correspond to the limit $\xi \to 0$.

Expanding (3.15) for small ξ, we obtain

$$\bar{w}_0 = F(z) - F'(z)F(z)\eta\bar{x} + \ldots \tag{3.16}$$

It therefore follows from (3.2) and (3.3) that (3.9) becomes identical to (3.27) when, as yet, the undetermined function F is taken to be

$$F(z) = -\frac{u_\infty'(z)}{a} \ . \tag{3.17}$$

Equation (3.3) shows that $\eta \to 1$ in the 'small' sublayer

$$\bar{y} \equiv \frac{y}{\delta} = O(1) \tag{3.18}$$

of the much thicker region $\eta = O(1)$. Equation (3.15) then becomes

$$\bar{w}_0 = F(z - \bar{x}\bar{w}_0) \qquad \text{for} \qquad \bar{y} = O(1) \ . \tag{3.19}$$

4. REMOVAL OF SINGULARITIES

It is well known that the 'water wave' solution (3.15) does not remain valid for all $\xi > 0$. In fact, differentiating (3.15), with respect to z, shows that

$$\frac{\partial \bar{w}_0}{\partial z} = \frac{F'}{1 + \xi F'} \ , \tag{4.1}$$

which becomes singular at $\xi = -1/F'$. Here, the prime denotes differentiation with respect to the entire argument and we can suppose without loss of generality that the initial singularity occurs on the $z = 0$ plane. This singularity occurs at the downstream location, say ξ_s, given by

$$\xi_s = \underset{\zeta}{\text{Min.}}\ \bar{g}(\zeta) \ , \tag{4.2}$$

where

$$\bar{g}(\zeta) \equiv -\frac{1}{F'(\zeta)} \ , \tag{4.3}$$

which means that $\bar{g}'$ should equal zero there (see fig. 2).

Then, holding ξ constant, expanding z in a Taylor series about the singular point, and using (4.1) yields

$$z = \frac{1}{2}\left(\frac{d^2 z}{d\bar{w}_0^2}\right)_{\bar{w}_s}\left(\bar{w}_0 - \bar{w}_s\right)^2 + \frac{1}{3!}\left(\frac{d^3 z}{d\bar{w}_0^3}\right)_{\bar{w}_s}\left(\bar{w}_0 - \bar{w}_s\right)^3 + \ldots \ , \tag{4.4}$$

where $\bar{w}_s$ is the limiting value of $\bar{w}_0$ at this point. Then since

$$\frac{d^2z}{d\bar{w}_0^2} = \frac{dz}{d\bar{w}_0}\frac{\partial}{\partial z}\frac{dz}{d\bar{w}_0} = -\frac{\bar{g}'}{\bar{F}'} \to 0 \tag{4.5}$$

this, together with (3.14), shows that

$$\bar{v}_0 \to -\frac{1}{3}\beta_s z^{-2/3} \tag{4.6}$$

and

$$\bar{w}_0 \to \bar{w}_s + \beta_s z^{1/3} , \tag{4.7}$$

as $z \to 0$ with $\xi = \xi_s$, where β_s is, of course, an order-one constant.

On the other hand, (3.13), (3.14), and (4.1) show that

$$\bar{v}_0 \to \frac{1}{\xi_s - \xi} \tag{4.8}$$

and

$$\bar{w}_0 \to \bar{w}_s - \frac{z}{\xi_s - \xi} , \tag{4.9}$$

as $\xi \to \xi_s$ with z held constant.

We now construct an appropriate local solution that removes this singularity, or at least delays its formation. The relevant scaling depends on whether or not $\bar{w}_s$ is equal to zero. For definiteness, we consider only the case, corresponding to our numerical example, where $\bar{w}_s = 0$. The first significantly different scaling occurs when

$$\bar{\xi} \equiv \frac{\xi - \xi_s}{\sigma} = O(1) . \tag{4.10}$$

Then equations (4.7) and (4.9), or equivalently (4.6) and (4.8), show that the appropriate 'z-scaling' is

$$\bar{z} \equiv \frac{z}{\sigma^{3/2}} = O(1) , \tag{4.11}$$

and in order to match with (4.7) to (4.9), via (3.7) to (3.10), the dependent variables must scale like

$$u = 1 + O(\varepsilon) \tag{4.12}$$

$$v = \frac{\varepsilon}{\sigma^2} e^{-\eta/\sigma} \eta \bar{v}_I(\bar{\xi}, \eta, \bar{z}) \tag{4.13}$$

$$w = \frac{\varepsilon}{\sigma^{1/2}} \eta \bar{w}_I(\bar{\xi}, \eta, \bar{z}) \tag{4.14}$$

and

$$p = \varepsilon^2 d(z) + \frac{1}{2}\left(\frac{\varepsilon\eta}{\sigma^2} e^{-\eta/\sigma}\right)^2 \bar{p}_I(\bar{\xi}, \eta, \bar{z}) \tag{4.15}$$

where $\bar{v}_I$, $\bar{w}_I$, and $\bar{p}_I$ remain of order one in the limit as $\varepsilon \to 0$ with $\bar{\xi}$, η, and $\bar{z}$ held fixed. Substituting into (3.5) and (3.6) and retaining only the lowest order terms now yields

$$\left(1 - \frac{\xi_s}{\eta} \bar{v}_I\right) \frac{\partial \bar{v}_I}{\partial \bar{\xi}} + \bar{v}_I^2 + \bar{w}_I \frac{\partial \bar{v}_I}{\partial \bar{z}} = -\bar{p}_I + \frac{\xi_s}{2\eta} \frac{\partial p_I}{\partial \bar{\xi}} , \tag{4.16}$$

$$\left(1 - \frac{\xi_s}{\eta} \bar{v}_I\right) \frac{\partial \bar{w}_I}{\partial \bar{\xi}} + \bar{w}_I \frac{\partial \bar{w}_I}{\partial \bar{z}} = 0 , \tag{4.17}$$

and

$$\bar{v}_I - \frac{\xi_s}{\eta} \frac{\partial \bar{v}_I}{\partial \bar{\xi}} + \frac{\partial \bar{w}_I}{\partial \bar{z}} = 0 , \tag{4.18}$$

which clearly generalizes (3.12) to (3.14). The new terms are, in the main, due to singularity line curvature effects.

Equations (4.17) and (4.18) can now be solved for $\bar{v}_I$ and $\bar{w}_I$ and the results used in (4.16) to determine $\bar{p}_I$. Equation (4.18) will automatically be satisfied if we introduce the generalized stream function $\bar{\Psi}$ by

$$\bar{w}_I = \bar{\Psi} - \frac{\xi_s}{\eta} \frac{\partial \bar{\Psi}}{\partial \bar{\xi}} , \tag{4.19}$$

and

$$\bar{v}_I = -\frac{\partial \bar{\Psi}}{\partial \bar{z}} . \tag{4.20}$$

Substituting these into (4.17) shows that $\bar{\Psi}$ is determined by

$$\left(1 + \frac{\xi_s}{\eta}\,\bar{\Psi}_{\bar{z}}\right)\frac{\partial}{\partial\bar{\xi}}\left(\bar{\Psi} - \frac{\xi_s}{\eta}\,\bar{\Psi}_{\bar{\xi}}\right) + \left(\bar{\Psi} - \frac{\xi_s}{\eta}\,\bar{\Psi}_{\bar{\xi}}\right)\frac{\partial}{\partial\bar{z}}\left(\bar{\Psi} - \frac{\xi_s}{\eta}\,\bar{\Psi}_{\bar{\xi}}\right) = 0\ , \qquad (4.21)$$

and in order to match with (4.6) to (4.9) we must require that

$$\bar{\Psi} \to -\frac{1}{2}\,\beta_s \bar{z}^{1/3} \qquad \text{as} \qquad \bar{z} \to \pm\infty \ \text{ with } \ \bar{\xi} \ \text{ fixed}, \qquad (4.22)$$

and

$$\bar{\Psi} \to \frac{\bar{z}}{\bar{\xi}} \qquad \text{as} \qquad \bar{\xi} \to -\infty \ \text{ with } \ \bar{z} \ \text{ fixed}, \qquad (4.23)$$

which clearly represent appropriate asymptotic solutions to (4.21).

5. THE BOUNDARY LAYER EXPANSION

Viscous effects must obviously come into play when y becomes sufficiently small. The boundary layer will initially be two dimensional with the cross flow effects producing only a linear perturbation (as in Toomre, 1960) until its thickness becomes of the order of the length scale $\lambda\delta$ introduced in the previous section. We therefore suppose that $\bar{y} = O(1)$, introduce the long streamwise length scale

$$L^* = -\frac{\lambda}{\varepsilon \ln \delta} \qquad (5.1)$$

and set

$$\lambda\delta = \frac{L^*}{\bar{R}}\ , \qquad (5.2)$$

where

$$R \equiv \frac{U_\infty L^*}{\nu} \qquad (5.3)$$

is the 'global' Reynolds number based on L^*. It follows that

$$\delta = \frac{1}{\left(R_\lambda \varepsilon \ln \frac{1}{\delta}\right)^{1/2}}\ , \qquad (5.4)$$

which, in view of (2.1), is consistent with our assumption (3.1) that $\delta \ll 1$.

We first consider the region where $O\left(\bar{x} - \xi_s\right)$ is greater than $O(\sigma)$.

5.1. The Early Three-Dimensional Region

In this part of the flow we expect the streamwise velocity

$$u = U(\bar{x},\bar{y},z) \tag{5.5}$$

to be $O(1)$ and in order to satisfy continuity we put

$$v = -\varepsilon\,\delta(\ln\delta)V \tag{5.6}$$

$$w = -\varepsilon(\ln\delta)W\ , \tag{5.7}$$

where V and W are, of course, assumed to remain $O(1)$ as $\varepsilon \to 0$. Equations (3.3), (3.10), and (3.18) suggest that

$$p = \varepsilon^2 d(z) + O(\varepsilon\,\delta\,\ln\delta)^2 \tag{5.8}$$

in this region.

Substituting these scalings into the Navier-Stokes equations yields the three-dimensional zero pressure gradient boundary layer equations

$$U\frac{\partial U}{\partial \bar{x}} + V\frac{\partial U}{\partial \bar{y}} + W\frac{\partial U}{\partial z} = \frac{\partial^2 U}{\partial \bar{y}^2} \tag{5.9}$$

$$U\frac{\partial W}{\partial \bar{x}} + V\frac{\partial W}{\partial \bar{y}} + W\frac{\partial W}{\partial z} = \frac{\partial^2 W}{\partial \bar{y}^2} \tag{5.10}$$

and

$$\frac{\partial U}{\partial \bar{x}} + \frac{\partial V}{\partial \bar{y}} + \frac{\partial W}{\partial z} = 0\ . \tag{5.11}$$

U must clearly go to unity as $\bar{y} \to \infty$ in order to match with (3.7). The boundary condition for W is a bit more subtle. The known properties of the boundary layer solutions suggest that the cross stream derivatives should become small as $\bar{y} \to \infty$. Equation (5.10) therefore becomes

$$\frac{\partial W}{\partial \bar{x}} + W\frac{\partial W}{\partial z} = 0\ , \tag{5.12}$$

whose solution is given by

$$W = G(z - \bar{x}W)\ . \tag{5.13}$$

This will clearly agree with (3.19) and (5.7) will therefore match with (3.9) if we take

$$G = F \ , \tag{5.14}$$

where F is given by (3.17). It is worth noting that the continuity equation (5.11) automatically insures that (5.6) will match with (3.8) and (3.14).

The appropriate boundary conditions for (5.9) to (5.11) are therefore

$$U \to 1, \ W \to F(z - \bar{x}W) \qquad \text{as} \qquad \bar{y} \to \infty \tag{5.15}$$

$$U = V = W = 0 \qquad \text{at} \ \ \bar{y} = 0 \ , \tag{5.16}$$

and since the cross flow effects become small as $\bar{x} \to 0$, U must go to the Blasius solution in this limit, i.e.,

$$U \to U_B(\bar{x},\bar{y}) \qquad \text{as} \qquad \bar{x} \to 0 \ . \tag{5.17}$$

The solution to this problem should, of course, become singular at the inviscid singular point ξ_s.

5.2. Terminal Form of Early Three-Dimensional Solution

It is first necessary to find the terminal asymptotic form of the solution to the initial boundary layer problems (5.9) to (5.11) in order to extend the boundary layer solution through the singularity. For simplicity, we again consider only the case, corresponding to our numerical example, where the cross flow velocity vanishes at the singularity.

We expect the solution to be of similarity form in the vicinity of the singular point ξ_s and the numerical results suggest that it develops a double layer structure with a thick, predominantly inviscid, outer region and a somewhat thinner viscous dominated sublayer. We therefore begin with the outer region, put

$$\tilde{y} = \left(\xi_s - \bar{x}\right)^{\gamma} \bar{y} \ , \tag{5.18}$$

and

$$\tilde{z} = \frac{z}{\left(\xi_s - \bar{x}\right)^{3/2}} \ , \tag{5.19}$$

with $\gamma > 0$ and seek a solution of the form

$$U = f(\tilde{y},\tilde{z}) \ , \tag{5.20}$$

$$V = \frac{g(\tilde{y},\tilde{z})}{\left(\xi_s - \bar{x}\right)^{\gamma+1}} \ , \tag{5.21}$$

and

$$W = \left(\xi_s - \bar{x}\right)^{1/2} h(\tilde{y},\tilde{z}) \ . \tag{5.22}$$

It follows from (5.9) to (5.11) that

$$-\frac{1}{2} fh + (g - \gamma\tilde{y}f)\frac{\partial h}{\partial \tilde{y}} + \left(h + \frac{3}{2}\tilde{z}f\right)\frac{\partial h}{\partial \tilde{z}} = 0 \ , \tag{5.23}$$

$$(g - \gamma\tilde{y}f)\frac{\partial f}{\partial \tilde{y}} + \left(h + \frac{3}{2}\tilde{z}f\right)\frac{\partial f}{\partial \tilde{z}} = 0 \ , \tag{5.24}$$

$$-\gamma\tilde{y}\frac{\partial f}{\partial \tilde{y}} + \frac{\partial g}{\partial \tilde{y}} + \frac{3}{2}\tilde{z}\frac{\partial f}{\partial \tilde{z}} + \frac{\partial h}{\partial \tilde{z}} = 0 \ . \tag{5.25}$$

The choice of γ will, in general, depend on the particular problem, but for the case, corresponding to our numerical example, where the singularity lies on a symmetry plane, h will behave like $h_0(\tilde{y})\tilde{z}$ and $\tilde{z}$-derivatives of f and g will vanish on this plane. It follows from (5.24) that either $\partial f/\partial \tilde{y}$ must vanish or

$$g = \gamma\tilde{y}f \ . \tag{5.26}$$

Our numerical results suggest the latter, and (5.25) therefore implies that

$$h_0 + \gamma f = 0 \ , \tag{5.27}$$

which will only be compatible with (5.23) if

$$\gamma = 1 \ , \tag{5.28}$$

which, in turn, shows that

$$h_0 = -f \qquad \text{on} \qquad z = 0 \ . \tag{5.29}$$

Equations (4.8) and (4.9) and the inviscid boundary conditions at the plate require that

$$f \to 1 \ , \tag{5.30}$$

$$h \to \tilde{k}(\tilde{z}) \ , \tag{5.31}$$

$$g \to -\tilde{y}\tilde{h}'(\tilde{z}) \ , \tag{5.32}$$

as $\tilde{y} \to \infty$ and

$$g \sim \tilde{y}^2 \qquad f \sim \tilde{y} \qquad \text{as} \qquad \tilde{y} \to 0 \ . \tag{5.33}$$

To find the viscous wall layer solution we put

$$\tilde{Y} = \left(\xi_s - \bar{x}\right)^{\alpha} \bar{y} \tag{5.34}$$

and seek a similarity solution of the form

$$U = \left(\xi_s - \bar{x}\right)^{1+2\alpha} F_w(\tilde{Y},\tilde{z}) \ , \tag{5.35}$$

$$V = \left(\xi_s - \bar{x}\right)^{\alpha} G_w(\tilde{Y},\tilde{z}) \ , \tag{5.36}$$

$$W = \left(\xi_s - \bar{x}\right)^{(3/2)+2\alpha} H_w(\tilde{Y},\tilde{z}) \ . \tag{5.37}$$

It therefore follows from (5.9) to (5.11) and (5.19) to (5.21) that

$$-(1 + 2\alpha)F_w^2 + (G_w - \alpha\tilde{Y}F_w)\frac{\partial F_w}{\partial \tilde{Y}} + \left(H_w + \frac{3}{2}\tilde{z}F_w\right)\frac{\partial F_w}{\partial \tilde{z}} = \frac{\partial^2 F_w}{\partial \tilde{Y}^2} \tag{5.38}$$

$$-\left(2\alpha + \frac{3}{2}\right)F_w H_w + (G_w - \alpha\tilde{Y}F_w)\frac{\partial H_w}{\partial \tilde{Y}} + \left(H_w + \frac{3}{2}\tilde{z}F_w\right)\frac{\partial H_w}{\partial \tilde{z}} = \frac{\partial^2 H_w}{\partial \tilde{Y}^2} \ , \tag{5.39}$$

and

$$-(1 + 2\alpha)F_w - \alpha\tilde{Y}\frac{\partial F_w}{\partial \tilde{Y}} + \frac{\partial G_w}{\partial \tilde{Y}} + \frac{3}{2}\tilde{z}\frac{\partial F_w}{\partial \tilde{z}} + \frac{\partial H_w}{\partial \tilde{z}} = 0 \ . \tag{5.40}$$

Matching with (5.20) to (5.22) and (5.33) requires that

$$F_w \sim \tilde{Y}, \qquad G_w \sim \tilde{Y}^2 \ , \tag{5.41}$$

as $\tilde{Y} \to \infty$, and

$$\alpha = 0 \ . \tag{5.42}$$

The viscous wall conditions require that

$$F_w = G_w = H_w = 0 \qquad \text{at} \qquad \tilde{Y} = 0 \ . \tag{5.43}$$

It is worth noting that (5.38) to (5.40) have the exact symmetry plane solution

$$F_w = -\frac{\partial H_w}{\partial \tilde{z}} = \tilde{a}\tilde{Y} \; ; \qquad G_w = \tilde{a}\tilde{Y}^2 \qquad \text{for} \qquad \tilde{z} = 0 \; ,$$

where $\tilde{a}$ is a constant and that the wall shear must behave like

$$\left(\frac{\partial U}{\partial \tilde{Y}}\right)_{\tilde{Y}=0} = \tilde{\tau}(\tilde{z})(\xi_s - \bar{x}) \qquad \text{as} \qquad \bar{x} \to \xi_s \tag{5.44}$$

for all values of $\tilde{z}$.

5.3. The Inviscid Inner Solution

Close to the singularity, where $\xi - \xi_s = O(\sigma)$, the boundary layer solution must match onto the inner solutions (4.12) to (4.15) (rather than onto (3.19)) and onto the terminal forms (5.20) to (5.22) and/or (5.35) to (5.37) of the boundary layer solutions (5.5) to (5.7). Our preliminary investigation of the equations revealed that singularity line curvature continues to play an important role even in this relatively thin region. We therefore anticipate that the relevant solution will have a double layer structure and that in the upper layer will be of the form

$$u = U_I(\bar{\xi}, \bar{y}_I, \bar{z}) \; , \tag{5.45}$$

$$v = \frac{\varepsilon\delta_I}{\sigma^2} V_I(\bar{\xi}, \bar{y}_I, \bar{z}) \; , \tag{5.46}$$

$$w = \frac{\varepsilon}{\sigma^{1/2}} W_I(\bar{\xi}, \bar{y}_I, \bar{z}) \; , \tag{5.47}$$

and

$$p = \varepsilon^2 d(z) + O\left(\varepsilon\delta_I\right)^2 \; ,$$

where

$$\bar{y}_I \equiv \frac{y}{\delta_I} \tag{5.48}$$

and, in order to match with (5.20) to (5.22) we must take

$$\delta_I = \frac{\delta}{\sigma} \; . \tag{5.49}$$

Substituting these into the Euler equations (viscous effects are, of course, negligible on the short streamwise length scale (4.4)) we obtain

$$U_I \frac{\partial U_I}{\partial \bar{\xi}} + V_I\left(\frac{\partial}{\partial \bar{y}_I} - \frac{\xi_s}{\bar{y}_I}\frac{\partial}{\partial \bar{\xi}}\right)U_I + W_I \frac{\partial U_I}{\partial \bar{z}} = 0 \ , \tag{5.50}$$

$$U_I \frac{\partial W_I}{\partial \bar{\xi}} + V_I\left(\frac{\partial}{\partial \bar{y}_I} - \frac{\xi_s}{\bar{y}_I}\frac{\partial}{\partial \bar{\xi}}\right)W_I + W_I \frac{\partial W_I}{\partial \bar{z}} = 0 \ , \tag{5.51}$$

and

$$\frac{\partial U_I}{\partial \bar{\xi}} + \left(\frac{\partial}{\partial \bar{y}_I} - \frac{\xi_s}{\bar{y}_I}\frac{\partial}{\partial \bar{\xi}}\right)V_I + \frac{\partial W_I}{\partial \bar{z}} = 0 \ . \tag{5.52}$$

U_I must clearly go to unity in order to match with (4.12). Matching with (4.13) and (4.14) can also be enforced if, as we might anticipate from the properties of the thin layer equations, W_I becomes independent of $\bar{y}_I$ as $\bar{y}_I \to \infty$. Then V_I will behave like $\bar{y}_I V_{I,0}(\bar{\xi},\bar{z})$ where $V_{I,0}$ and W_I then satisfy

$$(1 - V_{I,0}\xi_s)\frac{\partial W_I}{\partial \bar{\xi}} + W_I \frac{\partial W_I}{\partial \bar{z}} = 0 \tag{5.53}$$

and

$$V_{I,0} - \xi_s \frac{\partial V_{I,0}}{\partial \bar{\xi}} + \frac{\partial W_I}{\partial \bar{z}} = 0 \tag{5.54}$$

as $\bar{y}_I \to \infty$, which is clearly compatible with (4.17) and (4.18). The inviscid wall condition, of course, requires that

$$V_I = 0 \qquad \text{at} \qquad \bar{y}_I = 0 \ , \tag{5.55}$$

and we anticipate that U_I and W_I will also go to zero there.

Matching with the upstream solutions (5.20) to (5.22) requires that

$$U_I \to f\left(-\bar{\xi}\bar{y}_I, \frac{\bar{z}}{(-\bar{\xi})^{3/2}}\right) \ , \tag{5.56}$$

$$W_I \to (-\bar{\xi})^{1/2} h\left(-\bar{\xi}\bar{y}_I, \frac{\bar{z}}{(-\bar{\xi})^{3/2}}\right) \ , \tag{5.57}$$

etc., as $\bar{\xi} \to -\infty$.

5.4. The Viscous Wall Layer

The expansions (5.45) to (5.47) does not, of course, remain valid in the region near the wall where $\bar{y}_I \to 0$. However, the scalings (4.10) and (4.11) should still hold and the upstream solutions (5.35) to (5.37) suggest that u and w will be $O(\sigma)$ and $O(\sigma^{1/2}\varepsilon)$ there. The viscous terms will then be of the same order as the convection terms when $\bar{y} = O(1)$ and it follows from the requirements of continuity that the wall layer solution should scale like

$$u = \sigma \bar{U}_I(\bar{\xi},\bar{y},\bar{z}) \ , \tag{5.58}$$

$$v = \frac{\varepsilon\delta}{\sigma} \bar{V}_I(\bar{\xi},\bar{y},\bar{z}) \ , \tag{5.59}$$

$$w = \varepsilon\sigma^{1/2} \bar{W}_I(\bar{\xi},\bar{y},\bar{z}) \ , \tag{5.60}$$

Then the Navier-Stokes equations show that the order-one quantities $\bar{U}_I$, $\bar{V}_I$, $\bar{W}_I$ are determined by

$$\left[\bar{U}_I \frac{\partial}{\partial\bar{\xi}} + \bar{V}_I\left(\frac{\partial}{\partial\bar{y}} - \frac{\xi_s}{\bar{y}} \frac{\partial}{\partial\bar{\xi}}\right) + \bar{W}_I \frac{\partial}{\partial\bar{z}} - \left(\frac{\partial}{\partial\bar{y}} - \frac{\xi_s}{\bar{y}} \frac{\partial}{\partial\bar{\xi}}\right)^2\right]\{\bar{U}_I,\bar{W}_I\} = 0 \ , \tag{5.61}$$

$$\frac{\partial\bar{U}_I}{\partial\bar{\xi}} + \left(\frac{\partial}{\partial\bar{y}} - \frac{\xi_s}{\bar{y}} \frac{\partial}{\partial\bar{\xi}}\right)\bar{V}_I + \frac{\partial\bar{W}_I}{\partial\bar{z}} = 0 \ , \tag{5.62}$$

subject to the viscous wall conditions

$$\bar{U}_I = \bar{V}_I = \bar{W}_I = 0 \qquad \text{at} \qquad \bar{y} = 0 \ , \tag{5.63}$$

and matching with (5.45) to (5.47) requires that $\bar{U}_I$ and $\bar{W}_I$ behave like

$$\bar{W}_I, \bar{U}_I \sim \bar{y} \qquad \text{as} \qquad \bar{y} \to \infty \ . \tag{5.64}$$

Matching with the upstream solutions (5.35) to (5.37) requires that,

$$\bar{U}_I \to -\bar{\xi} F_w\left(\bar{y}, \frac{\bar{z}}{(-\bar{\xi})^{3/2}}\right) \ , \tag{5.65}$$

$$\bar{W}_I \to (-\bar{\xi})^{3/2} H_w\left(\bar{y}, \frac{\bar{z}}{(-\bar{\xi})^{3/2}}\right) , \tag{5.66}$$

etc., as $\bar{\xi} \to -\infty$.

Figure 3 summarizes the overall asymptotic structure of the problem developed in this and the preceding sections.

6. NUMERICAL SOLUTION OF THE BOUNDARY LAYER PROBLEM

The three-dimensional boundary layer problems (5.9) to (5.11) with (5.15) to (5.17) was solved numerically using the Keller box method (Keller and Cebeci, 1972, Cebeci and Smith, 1974, and Cebeci, Khattab, and Stewartson, 1981).

To formulate the numerical problem we first introduce the Blasius variable $\tilde{\eta} = \bar{y}/\sqrt{\bar{x}}$ and write the boundary layer equations as a system of first-order differential equations

$$p' + ep = \bar{x}\left(U \frac{\partial U}{\partial \bar{x}} + W \frac{\partial W}{\partial z}\right) , \qquad q' + eq = \bar{x}\left(U \frac{\partial W}{\partial \bar{x}} + W \frac{\partial W}{\partial z}\right) \tag{6.1}$$

$$U' = p, \qquad W' = q \tag{6.2}$$

$$e' = \frac{U}{2} + \bar{x}\left(U \frac{\partial U}{\partial \bar{x}} + W \frac{\partial W}{\partial z}\right) , \tag{6.3}$$

where $' \equiv \partial/\partial\tilde{\eta}$.

The boundary conditions are given by equations (5.15) to (5.17) and

$$e(\bar{x}, \tilde{\eta} = 0, z) = 0 . \tag{6.4}$$

Note that the definition of e here differs from that used by Cebeci et al. (1981) to avoid an apparent singularity in (6.3) as $\bar{x} \to 0$.

A Fourier spectral decomposition (truncated to a finite number of terms) is now introduced in the spanwise direction as

$$U(\bar{x}, \tilde{\eta}, z) = \sum_{n=-N}^{N} u_n(\bar{x}, \tilde{\eta}) e^{inz} , \tag{6.5}$$

and similarly for the other variables where $u_{-n} = u_n^*$, etc. with $*$ indicating the complex conjugate.

The differential equations for the Fourier components then become

$$p_n' + \sum_{n=-N}^{N} p_m e_{n-m} = \bar{x}\left[\sum_{n=-N}^{N} u_m \frac{\partial u_{n-m}}{\partial \bar{x}} + \sum_{n=-N}^{N} i(n-m) w_m u_{n-m}\right] , \qquad (6.6)$$

$$q_n' + \sum_{n=-N}^{N} q_m e_{n-m} = \bar{x}\left[\sum_{n=-N}^{N} u_m \frac{\partial w_{n-m}}{\partial \bar{x}} + \sum_{n=-N}^{N} i(n-m) w_m w_{n-m}\right] , \qquad (6.7)$$

$$u_n' = p_n, \qquad w_n' = q_n , \qquad (6.8)$$

$$e_n' = \frac{u_n}{2} + \bar{x}\left(\frac{\partial u_n}{\partial \bar{x}} + i n w_n\right) , \qquad (6.9)$$

for $-N \le n \le N$.

The standard Keller box scheme is then applied to the equations for the Fourier components in the same way as described by Cebeci et al. (1981) to advance the solution downstream from an upstream station where the solution is known. To begin the calculation starting conditions are derived by expanding the boundary layer solution about the Blasius solution as $\bar{x} \to 0$. These expansions yield

$$U \sim \bar{f}' + \frac{1}{2} \tilde{\eta} \bar{f}'' F(z) \bar{x} \qquad (6.10)$$

$$V \sim -\frac{1}{2\sqrt{\bar{x}}} (\bar{f} - \tilde{\eta}\bar{f}') + \frac{1}{4} (\tilde{\eta}^2 \bar{f}'' - \bar{f} - 3\tilde{\eta}\bar{f}') F'(z) \sqrt{\bar{x}} \qquad (6.11)$$

and

$$W \sim \bar{f}' F(z) \qquad (6.12)$$

where $\bar{f} = \bar{f}(\tilde{\eta})$ is the Blasius function. The starting conditions for p, q, and e follow from these and (6.2) and (6.3).

A nonuniform mesh is used in the cross stream coordinate such that the J mesh points are distributed according to

$$\tilde{\eta}_0 = 0; \quad \tilde{\eta}_j = h_1 \frac{K^j - 1}{K - 1} , \quad j = 1, J . \qquad (6.13)$$

This has the effect of increasing the local mesh size from its smallest value near the wall, h_1, by a fixed percentage (prescribed by the constant K) for each subsequent box.

The introduction of the finite difference approximations yields a $5(2N + 1)$ by $5(2N + 1)$ nonlinear system of equations for the unknown Fourier coefficients at each cross stream grid point. The nonlinear system is linearized about a previous iteration (or initial guess) by Newton's method. The difference between two iterations is solved for in an efficient way by the block tridiagonal procedure until convergence is achieved. Products are evaluated in physical space and then transformed back to Fourier space using a standard Fast Fourier Transform algorithm.

An advantage to using the Fourier spectral decomposition rather than a marching procedure in the spanwise direction is that the need to modify the procedure when the cross flow velocity component changes sign (as will happen in the cases of interest here) is avoided. The spectral method maximizes communication in the cross flow variable which then takes on an elliptic nature as suggested by Dywer (1981).

7. RESULTS AND DISCUSSION

Since vorticity is carried by the fluid particles in an inviscid flow, vortex lines that are perpendicular to the plate at upstream infinity become infinitely elongated as they pass over the plate-leading to infinite velocities and infinitesimal length scales that can only be eliminated by viscous effects. This vortex stretching produces the logarithmic singularity in the initial linear inviscid solution which, incidentally, is well known in classical rapid distortion theory literature (Hunt and Carruthers, 1990). The nonlinear singularity is new but is also related to this vortex stretching mechanism. It is therefore not surprising that its formation is associated with the development of small spanwise length scales.

The solution to the three-dimensional boundary layer problem (5.9) to (5.11) and (5.15) to (5.17) depends only on the single function

$$F(z) = - \frac{u_\infty'(z)}{a} , \tag{7.1}$$

which characterizes the scaled upstream disturbance field with the constant a being determined by the local potential flow in the vicinity of the forward stagnation point. It can easily be scaled out of the problem by replacing ε by $a\varepsilon$ in (5.1), (5.4), (5.6), and (5.7).

Our interest is primarily in periodic-type disturbance fields, and for definiteness we choose

$$u_\infty = \cos z . \tag{7.2}$$

The initial singularity will then lie at

$$\xi_s = 1 \ . \tag{7.3}$$

The choice (7.2) has special symmetry properties which may tend to make our results less than universal. In particular, it forces the singularity to lie on a symmetry plane of the flow which may simplify the terminal asymptotic structure of the boundary layer solution. However, these issues are beyond the scope of the present work and will be deferred to a subsequent paper.

The characteristic streamwise length scale L^* of the boundary layer flow is given by

$$L^* = - \frac{2\lambda}{a\varepsilon \ \ln \sqrt{R_\lambda \varepsilon a}} \ , \tag{7.4}$$

when this quantity is renormalized to absorb a into the scaling. The boundary layer singularity therefore develops on this scale which means that it occurs further downstream (relative to the characteristic length scale λ of the disturbance) as the characteristic amplitude ε of the upstream disturbance and the leading edge/disturbance scale Reynolds number R_λ decrease. R_λ must, of course, always remain large in order for our analysis to be valid. The effect of the leading edge geometry is accounted for by the factor a.

The upstream boundary layer flow is predominantly two dimensional and there is an overlap region (in which $\bar{x} << 1$ and $x >> 0$) where it is given by the Blasius solution. This solution is therefore the appropriate upstream boundary condition for the $\bar{x}$-scale boundary layer problem under discussion. The computed streamwise velocity profiles are shown in figure 4. They clearly show the order-one change in the mean profile shape produced by the small cross flow velocity in the external stream. Benney (1984) was among the first to show that asymptotically small modulations occurring on sufficiently short length scales can lead to order-one changes in the mean flow. However, Benney's modulations arose from interacting Tollmein-Schlichting waves and are fundamentally different from the steady upstream distortion effects being considered herein.

The velocity profiles of figure 4 also point to the anticipated localized thickening of the boundary layer in the vicinity of the symmetry plane as $\bar{x} \to 1$ and to the associated reduction in spanwise length scale. Figure 5 is a plot of the upwash velocity profiles. The dramatic local increase in this velocity component might be described as a kind of 'bursting phenomena' which, up to now, has only been found in unsteady flows. This might lead to a local transition of the boundary layer and therefore provide a possible mechanism for by-pass transition. The answer to this question depends on the stability of the solution to the local rescaled boundary layer problems (5.41) to (5.48) and (5.54) to (5.59). The final resolution of this issue is therefore beyond the scope of the present work and will be pursued in a forthcoming paper.

The cross flow velocity vectors are plotted in figure 6. They show that the large upwash velocity is produced by a spanwise flow into the symmetry plane.

The boundary layer solution develops a double layer structure and the terminal form of this solution is given by (5.20) to (5.25) in the upper inviscid region whose thickness increases like

$$\frac{1}{1 - \bar{x}} \qquad \text{as} \qquad \bar{x} \to 1 \ , \tag{7.5}$$

and by (5.35) to (5.40) in the lower viscous region, whose thickness remains $O(1)$ as $\bar{x} \to 1$.

This solution becomes particularly simple on the symmetry plane where it implies that

$$U = f(\tilde{y},0) \ , \tag{7.6}$$

$$\frac{dW}{dz} = - \frac{f(\tilde{y},0)}{(1 - \bar{x})} \ , \tag{7.7}$$

and

$$V = \frac{\tilde{y} f(\tilde{y},0)}{(1 - \bar{x})^2} \ , \tag{7.8}$$

where the function f is indeterminate and has to be found from the numerical solution. The solution in the lower layer is still given by these formulas but with f equal to its asymptotic form

$$f = \tilde{a}\tilde{y} \ , \tag{7.9}$$

where $\tilde{a}$ is a constant. In this sense the lower layer is no longer a distinct asymptotic region but is part of the upper inviscid region to the order of approximation of the analysis. This, of course, only holds on the symmetry plane.

To obtain an accurate check on our terminal asymptotic solution we worked out the numerical solution to the symmetry plane boundary layer equations starting from the upstream Blasius solution. These equations can, of course, be solved independently of the flow in the rest of the boundary layer and are much simpler than the full three-dimensional equations. It turns out that (7.7) and (7.8) constitute an exact solution to these full equations and still satisfy the correct free-stream boundary condition, so that the numerical problem is especially simple in this case.

Figure 7(a) is a plot of the symmetry plane streamwise velocity profiles (at various values of $\bar{x}$) as a function of the composite singularity coordinate $\bar{y}(1 - \bar{x})/\sqrt{\bar{x}}$. It merely shows that the profiles go smoothly from their initial Blasius to their final asymptotic forms. Part (b) of this figure shows that

these profiles look quite different when plotted against the unscaled coordinate $\tilde{y}$ and again reflects the dramatic thickening of the boundary layer. The predicted linear behavior at the wall is also evident from this figure. The calculated wall shear stress is shown in figure 8. The asymptotic linear behavior and the ultimate vanishing of the wall shear, predicted by (5.44), is clearly verified by these results.

The vanishing of the wall shear at $\bar{x} = 1$ is indicative of the formation of a singularity in the boundary layer solution at this point. But since this singularity is directly related to the singularity in the outer inviscid solution, it is basically inviscid in nature and it is therefore not clear whether or not it is removable. The answer to this question depends on whether the local rescaled inviscid problems (4.12) to (4.18) and the corresponding local rescaled viscous problems (5.41) to (5.48) and (5.54) to (5.59) possess self consistent nonsingular solutions. This constitutes a very difficult numerical task that is beyond the scope of the present work. The nonremovability of the singularity would require that the upstream flow field predicted by our analysis be modified due to some form of boundary layer separation that would have to be accounted for in the initial formulation of the inviscid flow problem. This separation could, of course, be eliminated by terminating the plate before the singularity had a chance to form. But even if this is not done the strong local instability of the oncoming boundary layer profiles could promote transition upstream of singularity and again modify the flow before the singularity can occur. We therefore feel that it makes sense to investigate the stability of the upstream boundary layer profiles irrespective of whether or not the singularity is removable in the asymptotic sense.

We consider only the destabilization of the classical Tollmein-Schlichting waves, since these are likely to be the most unstable modes and it is consistent with our asymptotic approach to use the classical high Reynolds number asymptotic results given, for example, by Lin (1946) and Reid (1965, pp. 281-282). It is appropriate to use the asymptotic formulas associated with the lower branch of the neutral stability curve, since we are primarily interested in the initial development of the instability and it is not inconsistent with our scaling to assume that the Tollmein-Schlichting wavelength is short compared to λ. Then the mean flow can be treated as locally two dimensional for purposes of calculating the instability wave growth rates and since the most unstable profiles lie along the symmetry plane we consider only this portion of the flow.

The asymptotic instability wave growth rates depend only on the Reynolds number

$$R = \frac{U_\infty L^*}{\nu} ,$$

where L^* is given by (7.4), and the local wall shear and not on the detailed profile shape. We therefore used the wall shear from our symmetry plane boundary layer calculations in the classical Tollmein-Schlichting wave dispersion relations to generate the neutral stability curve shown in figure 9. We also show the neutral curve for the Blasius boundary layer instability waves at the

same streamwise location. Notice that the neutral stability curve moves well upstream of the Blasius curve.

Finally, we note that the present study bears some resemblance to the receptivity analyses of Goldstein (1983, 1985) and Goldstein, Leib, and Cowley (1987) in that is involves the internalization of free-stream disturbances with an attendent streamwise amplification of the perturbed boundary layer flow, but is differs from them in that it only involves changes in the mean flow and does not depend on the growth of local instability waves to produce the final effect.

ACKNOWLEDGMENT

The authors would like to thank Prof. A.F. Messiter of the University of Michigan for helpful discussions during the course of this work.

APPENDIX A

In this appendix we investigate the singular behavior of the drift function in the vicinity of the forward stagnation point where the complex potential $\tilde{W}$ behaves like

$$\tilde{W} \sim -\frac{a}{2} Z^2 \ , \tag{A-1}$$

and a is a real constant that is determined by matching with the 'outer' potential flow. It therefore follows from (2.5) that

$$\zeta = -aZ = -\sqrt{-2a\tilde{W}} \ , \tag{A-2}$$

and, consequently, that

$$|\zeta|^2 = 2a\sqrt{\Phi^2 + \Psi^2} \ . \tag{A-3}$$

Hence

$$\int \frac{d\Phi}{|\zeta|^2} = \int \frac{d\Phi}{U_0^2 + V_0^2} \sim \frac{1}{2a} \int \frac{d\Phi}{\sqrt{\Phi^2 + \Psi^2}} = -\frac{1}{2a} \ln\left(\sqrt{\Phi^2 + \Psi^2} - \Phi\right) \ . \tag{A-4}$$

It follows that

$$\Delta \sim -\frac{1}{a} \ln \Psi \qquad \text{as} \qquad \Psi \to 0 \qquad \text{when} \qquad \Phi > 0 \ . \tag{A-5}$$

REFERENCES

Agvawal, S., and Messiter, A.F. (1984) Turbulent Boundary-Layer Interaction with a Shock Wave at a Compression Corner. J. Fluid Mech., vol. 143, pp. 23-46.

Benny, D.J. (1984) The Evolution of Disturbances in Shear Flows at High Reynolds Numbers. Studies in Applied Mathematics, vol. 70, pp. 1-19.

Bush, W.B., On the Lagerstrom Mathematical Model for viscous Flow at Low Reynolds Number. SIAM, J. Appl. Math., vol. 20, no. 2, pp. 279-287.

Cebeci, T., Khattab, A.K., and Stewartson, K. (1981) Three-Dimensional Laminar Boundary Layers and the OK of Accessibility. J. Fluid Mech., vol. 107, pp. 57-87.

Cebeci, T., and Smith, A.M.O. (1974) Analysis of Turbulent Boundary Layers. Academic Press, New York.

Darwin, C. (1953) A Note on Hydrodynamics. Proc. Camb. Phil. Soc. 49, pp. 342-354.

Dwyer, H.A. (1981) Some Aspects of Three-Dimensional Laminar Boundary Layers. Ann. Rev. Fluid Mech., vol. 13, pp. 217-229.

Goldstein, M.E., The Evolution of Tollmein-Schlichting Waves Near a Leading Edge. J. Fluid Mech., vol. 127, pp. 59-81.

Goldstein, M.E. (1978) Unsteady Vortical and Entropic Distortions of Potential Flows Sound Arbitrary Obstacles. J. Fluid Mech., vol. 89, part 3, pp. 433-468.

Goldstein, M.E. (1979) Turbulence Generated by the Interaction of Entropy Fluctuations with Nonuniform Meanflows. J. Fluid Mech., vol. 93, part 2, pp. 209-224.

Goldstein, M.E. (1985) Scattering of Acoustic Waves into Tollmein-Schlichting Waves by Small Streamwise Variations in Surface Geometry. J. Fluid Mech., vol. 154, pp. 509-529.

Goldstein, M.E., Leib, S.J., and Cowley, S.J. (1987) Generation of Tollmein-Schlichting Waves on Interactive Marginally Separated Flows. J. Fluid Mech., vol. 181, pp. 485-517.

Goldstein, M.E., Sockol, P.M., and Sanz, J. (1983) The Evolution of Tollmein-Schlichting Waves Near a Leading Edge, Part 2. Numerical Determination of Amplitudes. J. Fluid Mech., vol. 129, pp. 443-453.

Hunt, J.C.R. and Carruthers, D.J. (1990) Rapid Distortion Theory and the 'Problems' of Turbulence. J. Fluid Mech., vol. 212, pp. 497-532.

Keller, H.B., and Cebeci, T. (1972) Accurate Numerical Methods for Boundary Layer Flows. AIAA Journal, vol. 10, no. 9, pp. 1193-1199.

Lagerstrom, P.A. and Casten, R.G., Basic Concepts Underlying Singular Perturbation Techniques. SIAM Review, vol. 14, no. 1, pp. 63-120.

Lighthill, M.J. (1956) Drift. J. Fluid Mech., vol. 1, pp. 31-53.

Lighthill, J.J. (1978) Waves in Fluid. Cambridge University Press.

Nayfeh, A.H. (1981) Effect of Streamwise Vortices on Tollmein-Schlichting Waves. J. Fluid Mech., 107, p. 441.

Toomre, A. (1960) The Viscous Secondary Flow Ahead of an Infinite Cylinder in a Uniform Parallel Shear Flow. J. Fluid Mech., vol. 7, pp. 145-155.

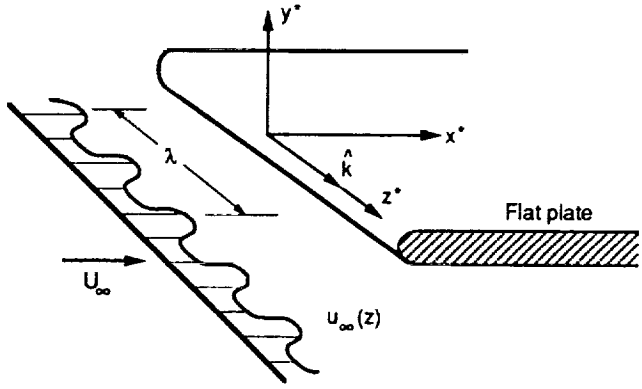

Figure 1.—Problem geometry.

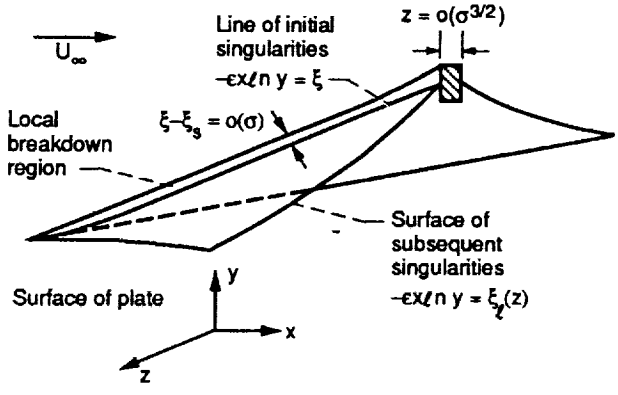

Figure 2.—Surface of inviscid singularities.

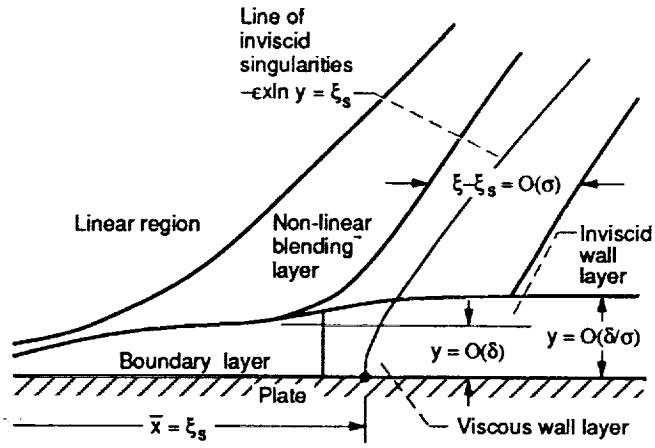

Figure 3.—Overview of asymptotic structure.

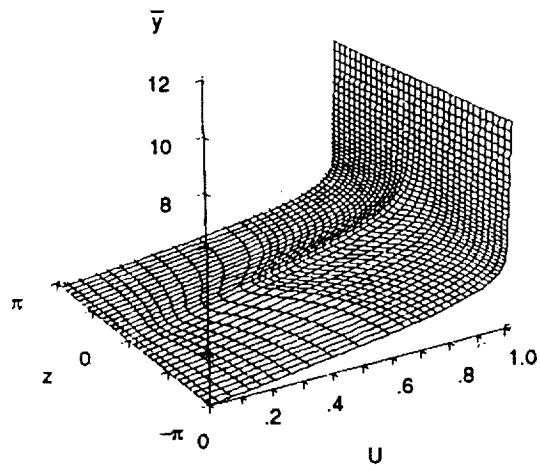

(a) $\bar{x} = 0.4$.

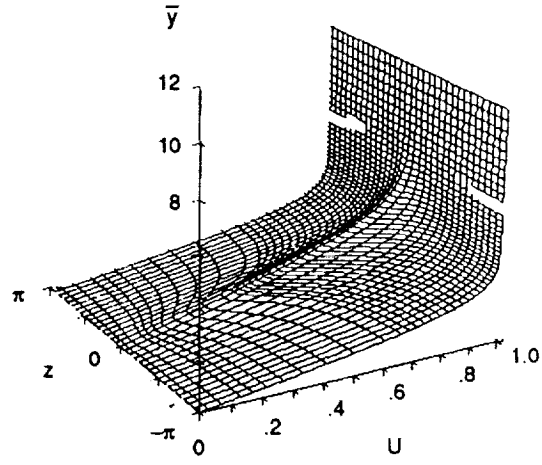

(b) $\bar{x} = 0.5$.

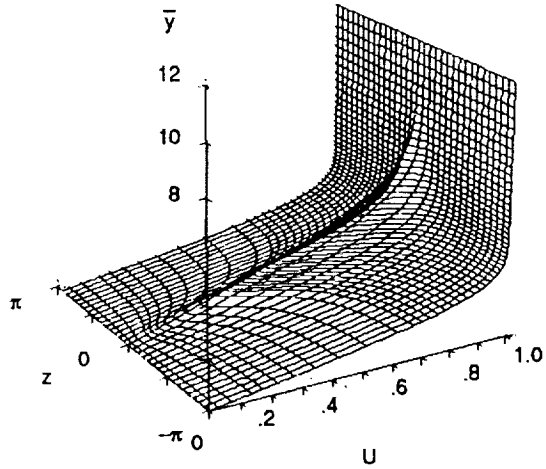

(c) $\bar{x} = 0.6$.

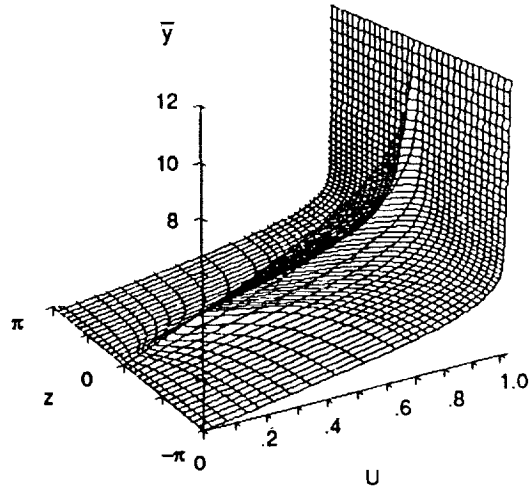

(d) $\bar{x} = 0.7$.

Figure 4.—Streamwise velocity profiles as a function of $\bar{y}$ and z.

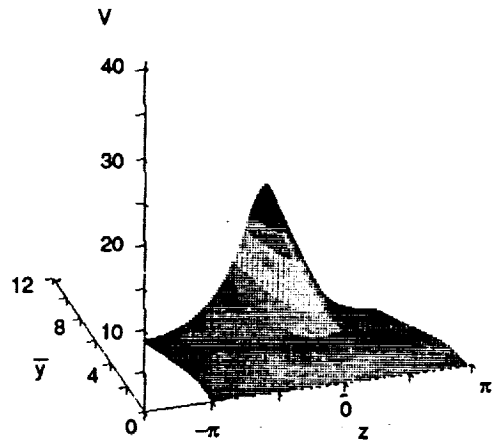

(a) $\bar{x} = 0.4$.

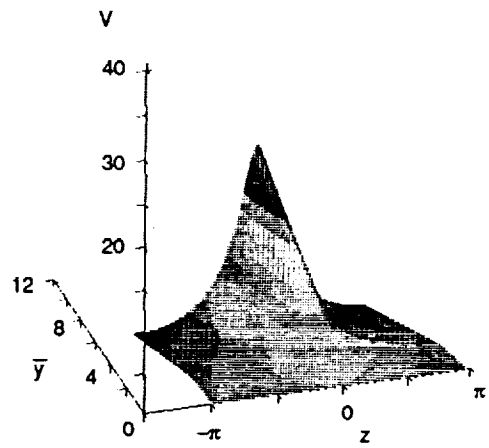

(b) $\bar{x} = 0.5$.

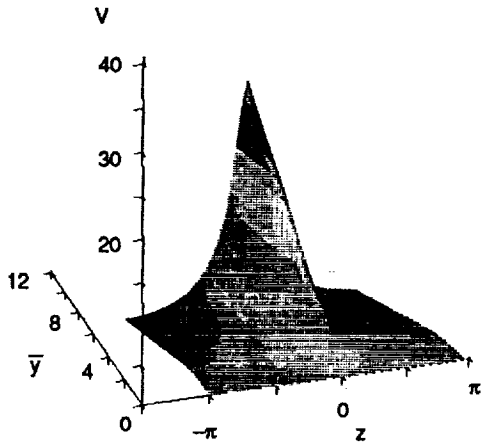

(c) $\bar{x} = 0.6$.

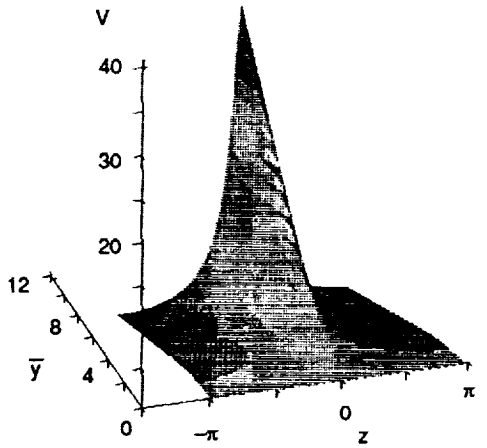

(d) $\bar{x} = 0.7$.

Figure 5.—Upwash velocity profiles as a function of $\bar{y}$ and z.

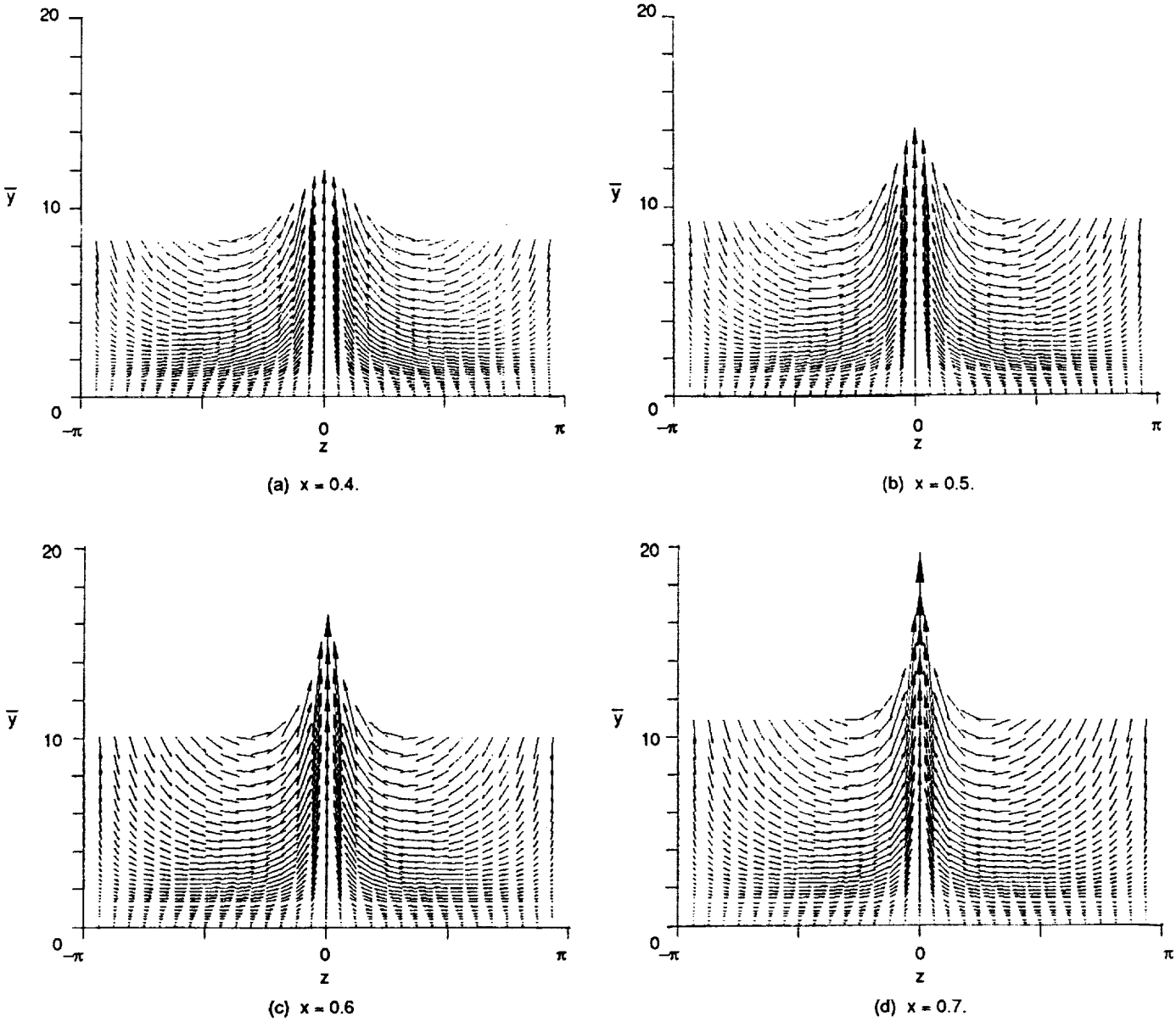

(a) x = 0.4.

(b) x = 0.5.

(c) x = 0.6

(d) x = 0.7.

Figure 6.—Velocity vectors in the crossflow plane.

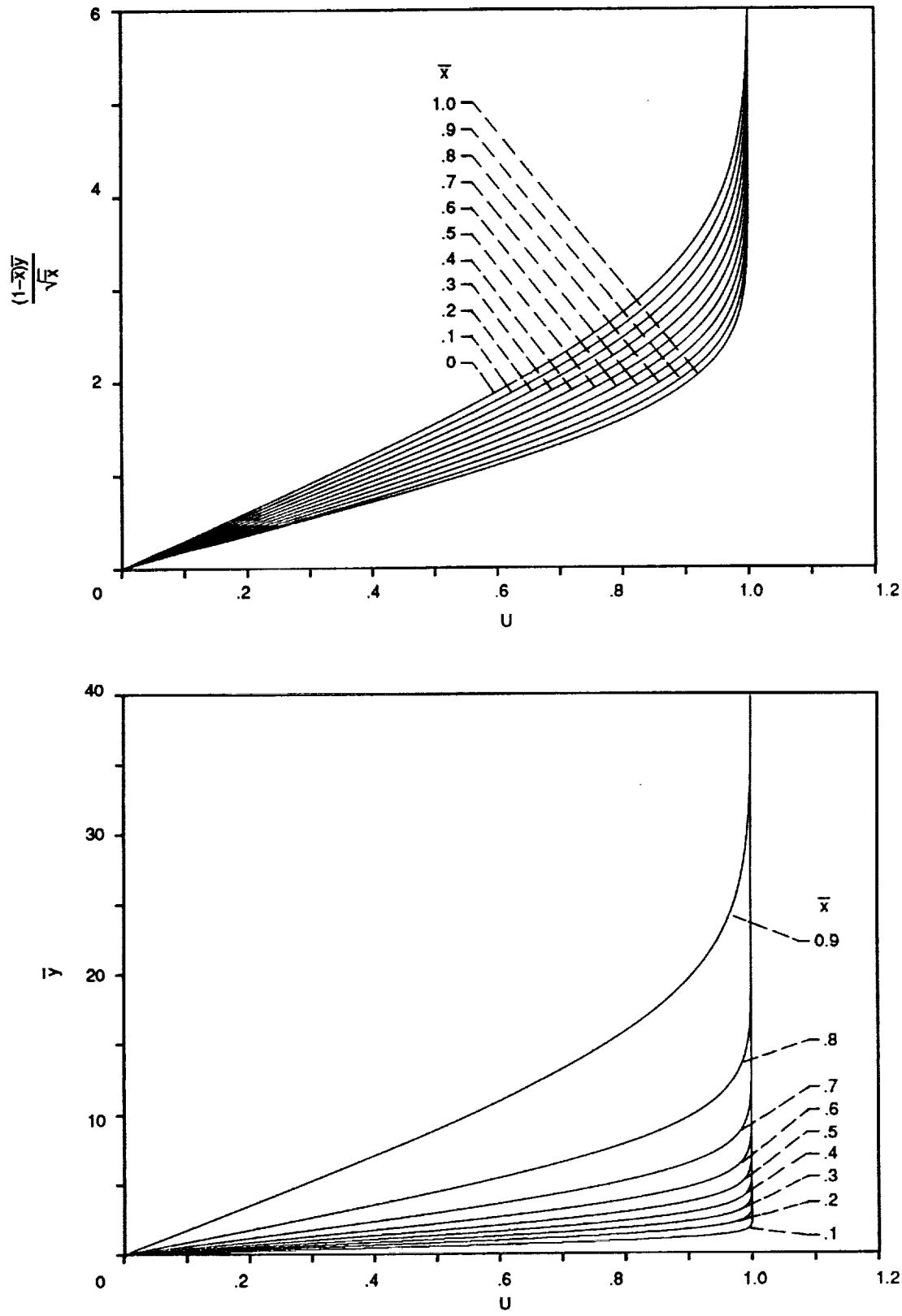

Figure 7.—Streamwise velocity profiles on the symmetry plane as a function of (a) $\bar{y}(1-\bar{x})/\sqrt{\bar{x}}$, and (b) $\bar{y}$ at various values of $\bar{x}$.

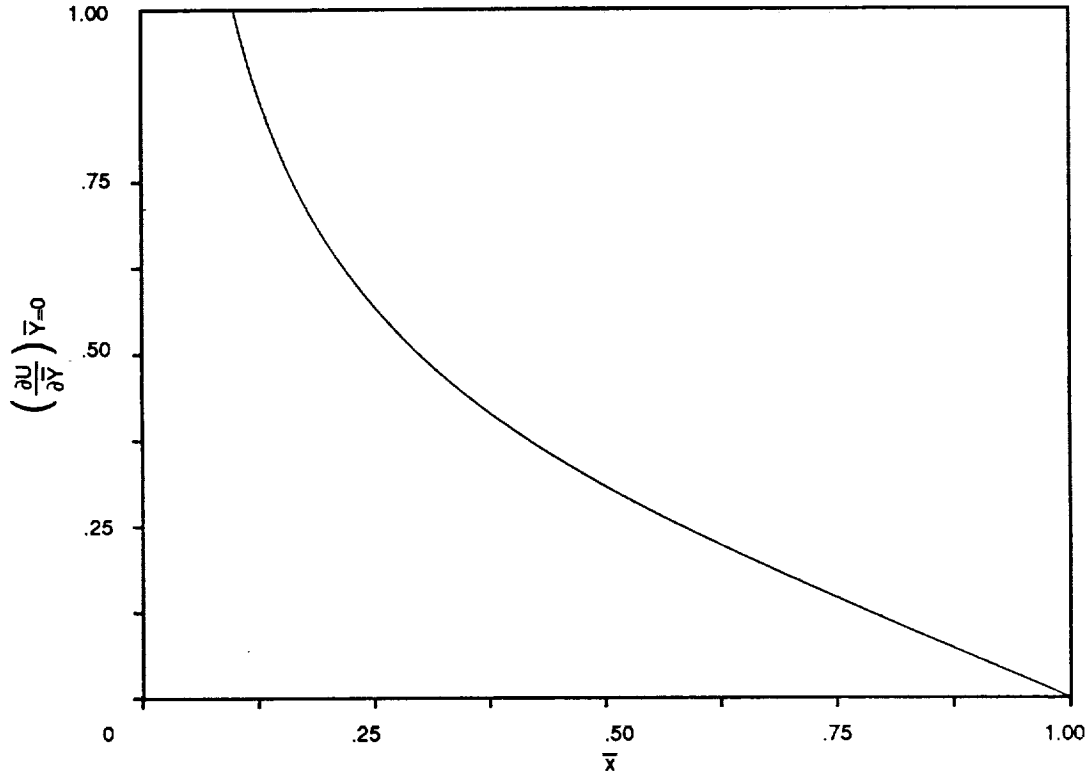

Figure 8.—Wall shear on symmetry plane as a function of $\bar{x}$.

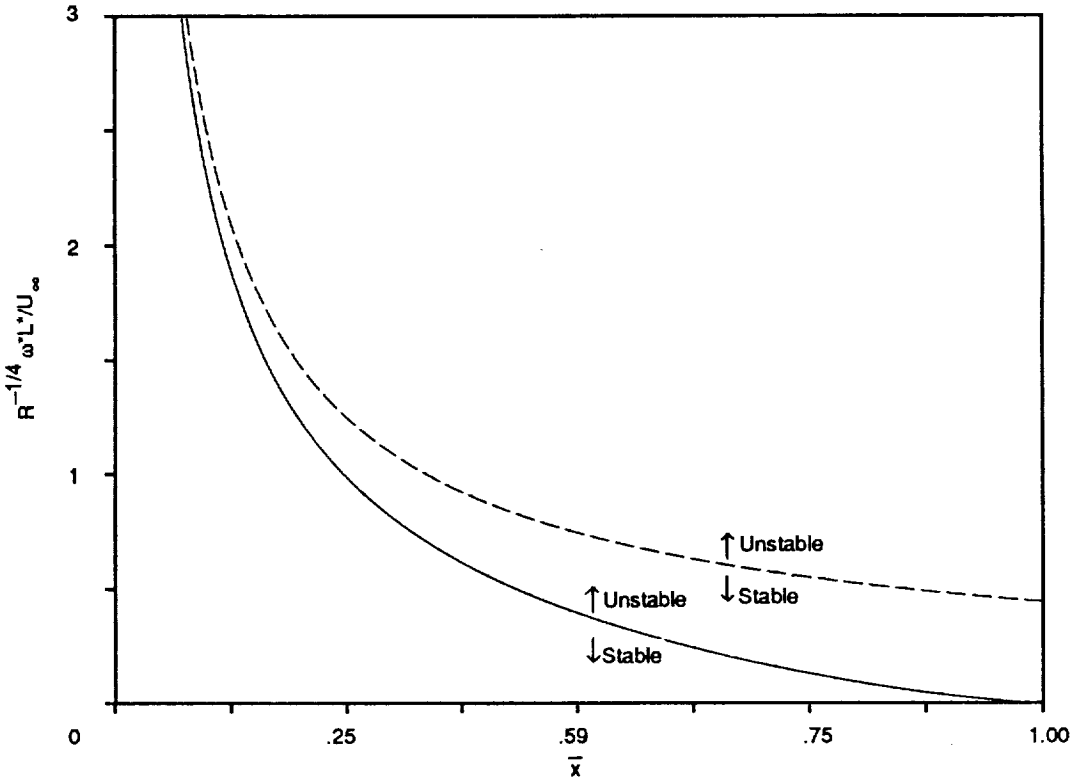

Figure 9.—Comparison of the lower branch of the neutral stability curve for the Blasius boundary layer (dashed curve) with that obtained using the computed wall shear on the symmetry plane.

NASA
National Aeronautics and Space Administration

Report Documentation Page

1. Report No.	2. Government Accession No.	3. Recipient's Catalog No.
NASA TM-103668 ICOMP-90-25		

4. Title and Subtitle

The Effect of Small Streamwise Velocity Distortion on the Boundary Layer Flow Over a Thin Flat Plate With Application to Boundary Layer Stability Theory

5. Report Date

December 1990

6. Performing Organization Code

7. Author(s)

M.E. Goldstein, S.J. Leib, and S.J. Cowley

8. Performing Organization Report No.

E-5759-1

10. Work Unit No

505-62-31

9. Performing Organization Name and Address

National Aeronautics and Space Administration
Lewis Research Center
Cleveland, Ohio 44135-3191

11. Contract or Grant No.

13. Type of Report and Period Covered

Technical Memorandum

12. Sponsoring Agency Name and Address

National Aeronautics and Space Administration
Washington, D.C. 20546-0001

14. Sponsoring Agency Code

15. Supplementary Notes

M.E. Goldstein, NASA Lewis Research Center; S.J. Leib, Sverdrup Technology, Inc., Lewis Research Center Group, 2001 Aerospace Parkway, Brook Park, Ohio 44142; S.J. Cowley, University of Cambridge, DAMTP, Silver St., Cambridge CB39EW, England and Institute for Computational Mechanics in Propulsion, Lewis Research Center.

16. Abstract

We show how an initially linear spanwise disturbance of the free-stream velocity field is amplified by leading edge bluntness effects and ultimately leads to a small amplitude but nonlinear spanwise motion far downstream from the edge. This spanwise motion is imposed on the boundary layer flow and ultimately causes an order-one change in its profile shape. The modified profiles are highly unstable and can support Tollmein-Schlichting wave growth wall upstream of the theoretical lower branch of the neutral stability curve for a Blasius boundary layer.

17. Key Words (Suggested by Author(s))	18. Distribution Statement
Three-dimensional boundary layers Boundary layer stability	Unclassified – Unlimited Subject Category 34

19. Security Classif. (of this report)	20. Security Classif. (of this page)	21. No. of pages	22. Price*
Unclassified	Unclassified	36	A03

NASA FORM 1626 OCT 86

*For sale by the National Technical Information Service, Springfield, Virginia 22161